NASA/TM—2011-217223 AIAA–2011–3801

Computational Analysis of a Low-Boom Supersonic Inlet

Rodrick V. Chima
Glenn Research Center, Cleveland, Ohio

November 2011

NASA STI Program . . . in Profile

Since its founding, NASA has been dedicated to the advancement of aeronautics and space science. The NASA Scientific and Technical Information (STI) program plays a key part in helping NASA maintain this important role.

The NASA STI Program operates under the auspices of the Agency Chief Information Officer. It collects, organizes, provides for archiving, and disseminates NASA's STI. The NASA STI program provides access to the NASA Aeronautics and Space Database and its public interface, the NASA Technical Reports Server, thus providing one of the largest collections of aeronautical and space science STI in the world. Results are published in both non-NASA channels and by NASA in the NASA STI Report Series, which includes the following report types:

- TECHNICAL PUBLICATION. Reports of completed research or a major significant phase of research that present the results of NASA programs and include extensive data or theoretical analysis. Includes compilations of significant scientific and technical data and information deemed to be of continuing reference value. NASA counterpart of peer-reviewed formal professional papers but has less stringent limitations on manuscript length and extent of graphic presentations.

- TECHNICAL MEMORANDUM. Scientific and technical findings that are preliminary or of specialized interest, e.g., quick release reports, working papers, and bibliographies that contain minimal annotation. Does not contain extensive analysis.

- CONTRACTOR REPORT. Scientific and technical findings by NASA-sponsored contractors and grantees.

- CONFERENCE PUBLICATION. Collected papers from scientific and technical conferences, symposia, seminars, or other meetings sponsored or cosponsored by NASA.

- SPECIAL PUBLICATION. Scientific, technical, or historical information from NASA programs, projects, and missions, often concerned with subjects having substantial public interest.

- TECHNICAL TRANSLATION. English-language translations of foreign scientific and technical material pertinent to NASA's mission.

Specialized services also include creating custom thesauri, building customized databases, organizing and publishing research results.

For more information about the NASA STI program, see the following:

- Access the NASA STI program home page at *http://www.sti.nasa.gov*

- E-mail your question via the Internet to *help@sti.nasa.gov*

- Fax your question to the NASA STI Help Desk at 443–757–5803

- Telephone the NASA STI Help Desk at 443–757–5802

- Write to:
  NASA Center for AeroSpace Information (CASI)
  7115 Standard Drive
  Hanover, MD 21076–1320

NASA/TM—2011-217223 AIAA–2011–3801

Computational Analysis of a Low-Boom Supersonic Inlet

Rodrick V. Chima
Glenn Research Center, Cleveland, Ohio

Prepared for the
29th Applied Aerodynamics Conference
sponsored by the American Institute of Aeronautics and Astronautics
Honolulu, Hawaii, June 27–30, 2011

National Aeronautics and
Space Administration

Glenn Research Center
Cleveland, Ohio 44135

November 2011

Trade names and trademarks are used in this report for identification only. Their usage does not constitute an official endorsement, either expressed or implied, by the National Aeronautics and Space Administration.

This work was sponsored by the Fundamental Aeronautics Program at the NASA Glenn Research Center.

Level of Review: This material has been technically reviewed by technical management.

Available from

NASA Center for Aerospace Information
7115 Standard Drive
Hanover, MD 21076–1320

National Technical Information Service
5301 Shawnee Road
Alexandria, VA 22312

Available electronically at http://www.sti.nasa.gov

Computational Analysis of a Low-Boom Supersonic Inlet

Rodrick V. Chima
National Aeronautics and Space Administration
Glenn Research Center
Cleveland, Ohio 44135

Abstract

A low-boom supersonic inlet was designed for use on a conceptual small supersonic aircraft that would cruise with an over-wing Mach number of 1.7. The inlet was designed to minimize external overpressures, and used a novel bypass duct to divert the highest shock losses around the engine. The Wind-US CFD code was used to predict the effects of capture ratio, struts, bypass design, and angles of attack on inlet performance. The inlet was tested in the 8-ft by 6-ft Supersonic Wind Tunnel at NASA Glenn Research Center. Test results showed that the inlet had excellent performance, with capture ratios near one, a peak core total pressure recovery of 96 percent, and a stable operating range much larger than that of an engine. Predictions generally compared very well with the experimental data, and were used to help interpret some of the experimental results.

I. Introduction

The low-boom supersonic inlet (LBSI) was designed by engineers at Gulfstream Aerospace Corporation (GAC) for use on a small aircraft that would cruise at a Mach number of 1.6 at 45,000 feet[1]. Two features of the inlet were designed to minimize external overpressures that would contribute to the sonic boom signature of the aircraft. First, the external cowl angle was kept small to minimize external shocks. Second, the inlet was designed to capture nearly 100 percent of the oncoming supersonic flow, thereby minimizing external flow spillage.

The inlet used an axisymmetric, relaxed isentropic compression centerbody design to decelerate the flow into a non-uniform terminal shock. The shock was weak at the centerbody to minimize shock/boundary-layer interaction, but it was stronger at the cowl.

The inlet had two concentric flow paths. The inner, or core, flow path led to the aerodynamic interface plane (AIP) where the engine would be attached. The outer, or bypass, flow path was designed to route the low momentum air from the strongest part of the normal shock around an engine and gearbox, and back to the nozzle stream. This dual-stream design improved core recovery by diverting the high shock losses near the cowl through the bypass duct, and also minimized external shocks by keeping the gearbox out of the freestream flow[2].

The LBSI was tested in the 8-ft by 6-ft Supersonic Wind Tunnel (SWT) at NASA Glenn Research Center (GRC) in the fall of 2010[3]. The tests were conducted by a team of researchers from GRC, GAC, the University of Illinois at Urbana-Champaign, and the University of Virginia. Two inlet designs were tested – the dual-stream design intended for an aircraft, and a simpler single-stream design intended for more detailed flow physics measurements and CFD validation. The single-stream inlet will be reported in other publications and is not discussed here. Both inlets were tested with and without flow control devices, including microramps and vane vortex generators on the centerbody. The flow control devices will also be reported elsewhere.

Research team members performed many CFD analyses of the two inlets before the test was started. The analyses were done with several different CFD codes and at different levels of fidelity, including:

- Design of the compression spike using a method of characteristics code[1],
- Axisymmetric analyses to refine the design and predict general performance trends[4],
- An analysis of the dual-stream inlet coupled to a Rolls-Royce fan to predict engine stability characteristics[5],
- 3-D analyses of the inlets including struts and bypass geometry (present work), and
- Analyses of the inlets with microramps and vane vortex generators [6, 7, 8].

This paper describes a 3-D CFD analysis of the dual-stream LBSI without flow control devices, and compares the results of the analysis with data from a wind tunnel test. The inlet and test are described briefly, and the CFD analysis is described in more detail. The analysis was performed before the test to estimate the performance of the inlet, and to investigate the effects of struts, bypass vanes, and angle of attack on performance. Here the results of

the analysis are compared to the experimental data, primarily to validate the predictions, and also to explain some of the experimental results that are not obvious from the data.

II. Dual-Stream Low-Boom Supersonic Inlet

Engineers at Gulfstream Aerospace Corporation have been investigating technologies that would enable the use of a small, low-boom supersonic aircraft. Their reference aircraft, (Ref. 1) was designed to cruise at 45,000 feet at a Mach number of 1.6, with an over-wing Mach number of 1.7. The aircraft would use radical aerodynamic shaping and a Quiet Spike[9] to minimize sonic boom. The inlets make up much of the frontal area of the aircraft, so they were designed carefully to minimize their contribution to the overall sonic boom characteristics. Axisymmetric, external-compression inlets were chosen for simplicity.

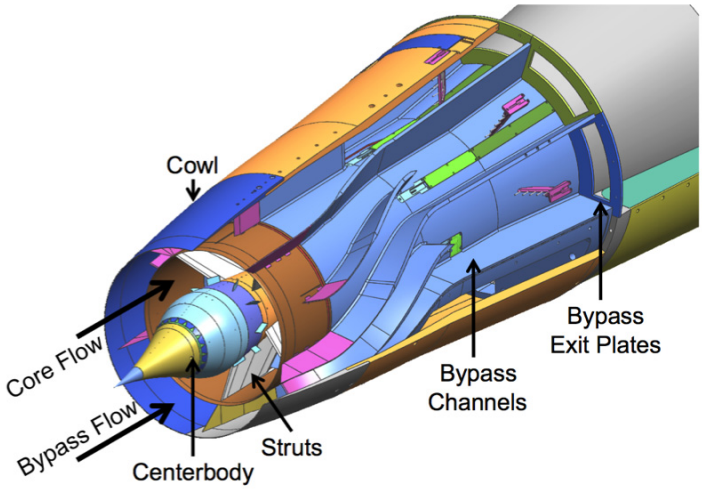

Figure 1. Dual stream inlet cutaway.

Reference 1 also describes an innovative approach for designing the external compression surface of the inlet that gives improved recovery and reduced sonic boom overpressures over conventional designs. Inlets designed with this approach have been tested experimentally[10] at small scale and modeled computationally[5, 11], and shown to have good recovery and stability characteristics.

In the present study a dual-stream inlet was designed using the approach described in Ref. 1. It was designed to reduce the Mach number from 1.7 over the wing to about 0.65 at the fan face, with high total pressure recovery, minimal distortion, and with minimal external overpressures. The inlet, shown in Figure 1, consists of a centerbody, a core flow stream, and a concentric bypass flow stream. Five thin struts connect the centerbody, bypass splitter, and cowl.

The centerbody consists of an isentropic compression spike, a curved throat region, and a subsonic diffuser (not visible in the figure). The compression spike was designed to produce a variable-strength normal shock at the throat. The Mach number ahead of the shock is about 1.3 near the centerbody, which is low enough to avoid boundary-layer separation. The Mach number at the cowl is close to the design over-wing value of 1.7, which generates a strong normal shock with high total pressure loss. After the shock the Mach number is reduced through the subsonic diffuser to 0.65 at the AIP.

The bypass duct was used to capture the high-loss flow near the cowl and divert it around the engine and back to the nozzle stream. This removes the high-loss flow from the core stream, and maximizes the total pressure recovery at the AIP. One of the goals of the present study was to demonstrate the performance and stability of an inlet with this type of a bypass duct.

In the test the bypass flow was throttled using five choked exit plates with annular slots that returned the bypass flow to the freestream. In an aircraft application the bypass duct would extend to the nozzle, and converging-diverging vanes would be used to expand the flow back to supersonic speeds.

The bypass duct can be used to keep the engine gearbox out of the external flow, where it would contribute to boom. The inlet considered here was sized for a Rolls-Royce Tay engine, which has a gearbox that extends almost 160 degrees around the perimeter. The bypass duct used 10 curved vanes to route the flow around the gearbox area. To maintain subsonic flow in the bypass duct it was necessary to increase the flow area downstream of the lip, which led to an eight-degree external cowl angle.

The bypass duct can also be used to divert separated flow from the sharp lip away from the core flow. Separation is a common problem with sharp-lipped supersonic inlets at low subsonic speeds and at angles of attack or yaw. In Ref. 5 it was shown that lip separation at low takeoff speeds could be contained in the bypass duct by blocking the duct exit. The present CFD work has shown that separation caused by high pitch or yaw angles is also diverted away from the core.

III. 8-ft by 6-ft Supersonic Wind Tunnel Test

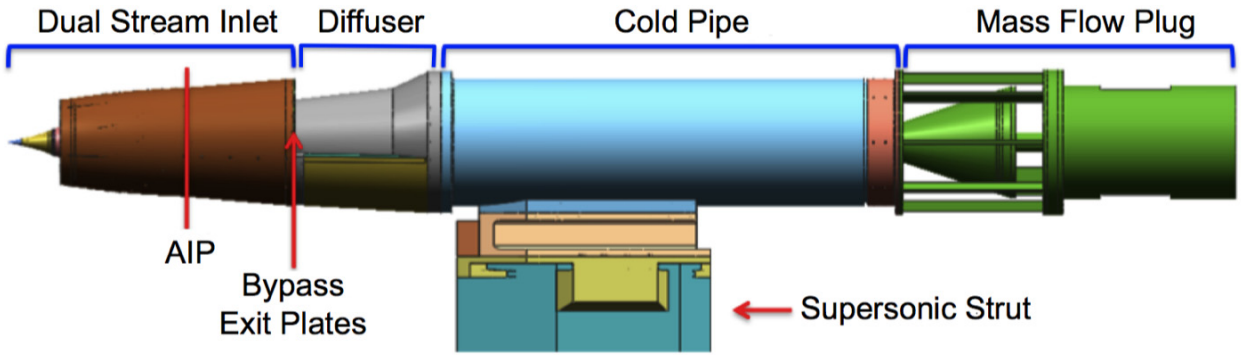

Figure 2. Dual-stream inlet model and support hardware.

The inlets were tested in the 8-ft by 6-ft SWT at NASA Glenn Research Center[12]. The test section of the tunnel is 8 feet high by 6 feet wide, and 23.5 feet long. The tunnel walls are perforated and surrounded by an evacuated balance chamber to remove the wall boundary layers. Large 26.5-inch diameter windows provided optical access to the test section, and a schlieren system was used to visualize the flow around the inlet. A high-speed Phantom V310 camera operating at 2000–4000 frames per second recorded steady or unsteady schlieren images.

For this test the tunnel was run in a closed-loop cycle, with the air passing through a dryer and a cooler to permit continuous operation. Data was taken at Mach numbers of 0.5 and 1.4 – 1.8. The SWT is an atmospheric tunnel that operates at high dynamic pressure and temperature. At $M = 1.8$ the tunnel total pressure is 23.2 psi and the total temperature is 631 R. The models and instrumentation were designed to handle these conditions.

Gulfstream engineers performed the initial aerodynamic and mechanical design of the model, and TriModels, Inc. in Huntington Beach, CA did the detailed design and fabrication. The model was instrumented with a total of 241 static or total pressure taps on the centerbody, cowl, two boundary-layer rakes, and eight AIP rakes. Standard SAE 1420 total pressure rakes[13] were located at the AIP, with eight five-probe rakes. A sixth probe was added to each rake near the hub to better resolve the hub boundary layers, which were expected to be large.

The dual-stream inlet model and the wind tunnel support hardware are shown in Figure 2. The model was mounted on a hydraulic strut that could be rotated to vary the angle of attack from -2 to +5 degrees. Yaw angles could not be varied.

The inlet core flow expanded through a subsonic diffuser into a 16-inch diameter cold pipe. The core flow was throttled using a hydraulically actuated conical mass flow plug (MFP) at the exit of the cold pipe. The MFP was calibrated to measure the core-stream mass flow rate to within a few tenths of a percent. The bypass channels were throttled using interchangeable choke plates at the channel exit. CFD was used before the test[4] to estimate the choke plate area needed to give the desired mass flow ratio of $\dot{m}_{bypass} / \dot{m}_{core} = 0.7$ at full capture. The choke plate area was verified by exchanging plates early in the test.

The dual-stream inlet had total pressure rakes at the exit of each bypass channel (Figure 1), with five probes in each rake. The mass flow through each channel was estimated using the average total pressure, the tunnel total temperature, and by assuming that $M = 1.0$ at the exit plate.

Inlet capture ratio compares the actual mass flow through the bypass and core to the maximum mass flow that the inlet could capture. Capture ratio is defined by

$$\text{capture ratio} = (\dot{m}_{core} + \dot{m}_{bypass}) / (\rho_\infty V_\infty \pi \, r_{cowl}^2)$$

The capture ratio was expected to be 1.0 at $M = 1.8$ when the MFP was wide open, but the measurements indicated a capture ratio of 1.145. The core mass flow was assumed to be accurate, so the bypass mass flow was reduced using a discharge coefficient $C_D = 1/1.145 = 0.873$. This C_D corrected the overall capture ratio to 1.0 at this condition, and the same C_D was used for all other operating conditions. Since C_D might vary with operating conditions, the accuracy of bypass flow rate measurement is uncertain.

IV. Computational Model

A. Differences Between Wind Tunnel Model and Flight (CFD) Inlet Designs

The computations shown later were made for flight hardware at altitude conditions, while the inlet that was tested in the SWT had differences in scale, flow conditions, strut chord, and bypass geometry. These differences, summarized in Table 1 and discussed below, were expected to have only minor effects on the comparison between the measured and computed results.

Table 1. Differences between wind tunnel model and flight (CFD) designs.

Parameter	SWT test	Flight (CFD)	Effects
Diameter	12 in. (1/4.86 scale)	58.4 in.	None
Mach number	1.664 nominal	1.7	Slight differences in shock angles
Re_D	5.2×10^6	12×10^6	Minimal
Strut size	4.75 in. chord at hub (scale size)	7.45 in. chord at hub	Differences in centerbody pressures and recovery behind struts
Bypass exit geometry	5 channels, diverging radius	1 channel, constant radius	Possible differences in secondary flow and losses

The CFD was performed for a 58.4-inch diameter inlet at 45,000 feet and $M = 1.7$. These conditions give a Reynolds number based on diameter of $\mathrm{Re}_D = 5.2\times10^6$. The test was performed on a 12-inch diameter ($1/4.86$ scale) model, in an atmospheric wind tunnel at $M = 1.664$ and $\mathrm{Re}_D = 12\times10^6$. Differences in freestream Mach number were accounted for by comparing pressure ratios or coefficients. Differences in Reynolds number were expected to be insignificant, since a sublimation technique used in the experiment showed that the centerbody boundary layer became fully turbulent very close to the leading edge.

Five swept struts were used to hold the centerbody in both the wind tunnel model and flight designs. The struts were tapered from hub to tip. The scaled leading edge locations of the two designs were identical, but the chord of the wind tunnel model was increased by 2.7 inches (13 inches flight scale) uniformly along the span. Thus, the flight strut had a scale hub chord of 4.75 inches and the wind tunnel model strut had a hub chord of 7.45 inches. This design change was unintended and was not discovered until after the test. The increase in chord length decreases the recovery measured downstream of the struts in the wind tunnel model. However, only one AIP rake was located directly behind a strut, so the effects on overall recovery are expected to be small. The struts had NACA profiles with $t/c = 0.04$, so the wind tunnel model had relatively more blockage between the struts. This increase in blockage causes centerbody pressures between the struts measured in the wind tunnel to be lower than pressures predicted by the CFD.

The flight inlet and wind tunnel model had identical bypass vanes near the leading edge. In the wind tunnel model (Figure 1) the vanes were thickened away from the leading edge, and every other vane was extended to the end of the bypass duct for structural reasons. Additionally, the hub and tip radii were increased in the plenum region to provide a favorable pressure gradient before the choke plates. In the flight inlet the bypass vanes stop at the end of the gearbox fairing, and the flows from the individual channels merge in a common, constant-area plenum region (compare Figures 2 and 4). These differences in bypass duct geometry probably create differences in secondary flows and pressure distributions in the plenum region, but they are not expected to affect the mass flow or recovery characteristics of the bypass duct.

B. Computational Grids

Computational grids for the inlet were generated using a combination of codes. Axisymmetric (x,r) grids for the core, bypass, and external flow were generated using Pointwise[14]. The core and external flow grids were rotated through 360 degrees using Pointwise, and the bypass grid was sheared between individual vanes using a custom code. The full, 360-degree inlet was modeled to allow calculations of yaw conditions. C-grids around the struts were generated using TCGRID[15]. The grid blocks were assembled using Pointwise, and converted to Wind-US[16] format using Gridgen[14]. Boundary conditions for Wind-US were applied using Gridgen and GMAN, one of the Wind-US utilities.

The computational grid is shown in Figures 3 – 5, which show the grid on the cowl, bypass vanes, and centerbody and struts, respectively. The final grid had about 24 million points in 25 blocks, as given in Table 2. The spacing at the walls was 1×10^{-5} inches, giving $y^+ = 1$ to 2 at the first point off the walls. Leading edges of the cowl, splitter, struts, and vanes were modeled as 2:1 ellipses, with 6-10 points along each surface, to give adequate resolution of bow shocks or incidence effects.

Grid refinement studies were done on the (x,r) grids in previous, unpublished work. The grids described in Table 2 were regenerated with about half as many points in each direction, while maintaining spacing at the walls. Axisymmetric calculations showed that recoveries predicted on the coarse grid were within 0.13 percent of the fine grid results, so the fine (x,r) grid used here was assumed to be adequate. Tangential grids had the same spacing at the wall and roughly square cells near passage centers. Tangential grid resolution was tested in Wind-US by running solutions with sequencing, in which every other grid point was used. Results with sequencing showed little difference between the coarse and fine grid solutions.

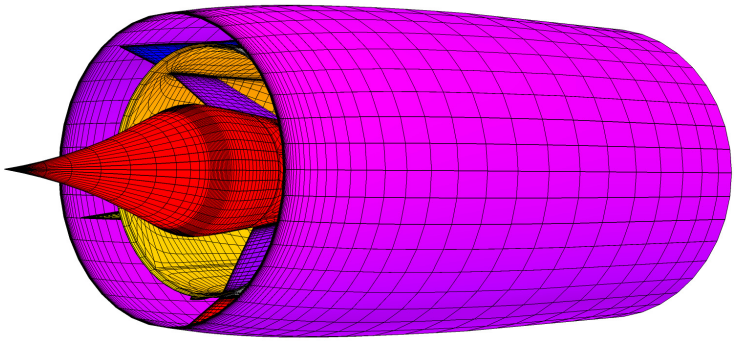

Figure 3. Computational grid on the cowl.

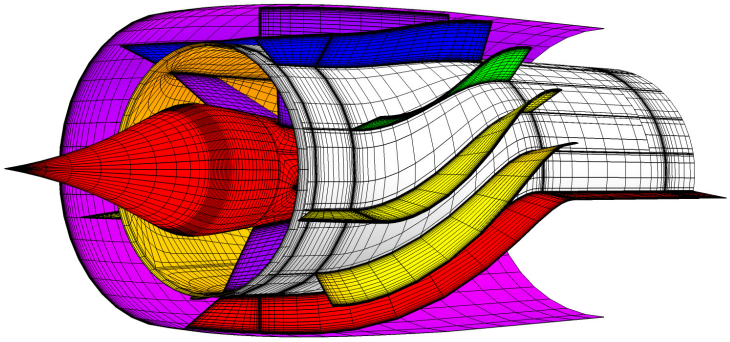

Figure 4. Computational grids on the bypass vanes.

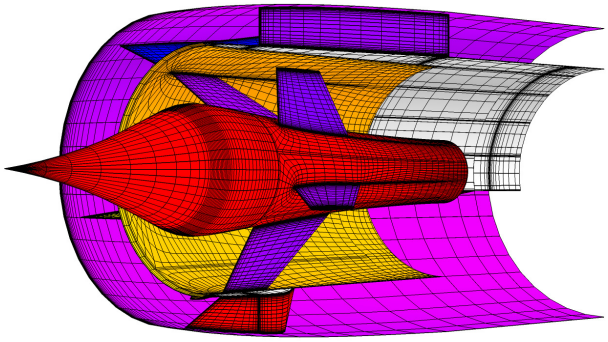

Figure 5. Computational grids on the centerbody and struts.

Table 2. Computational grid sizes for the inlet.

Region	Blocks	i	j	k	Points
Core	2	279	121	65	4,388,670
Bypass	2	274	121	45	2,983,860
External Flow	4	314	121	65	9,878,440
Struts	5	181	45	65	2,647,125
Core Exit	1	17	441	65	487,305
Bypass Channels	10	193	33	45	2,866,050
Bypass Exit	1	51	321	45	736,695
Totals	25				23,988,145

C. CFD Solution Scheme

The dual-stream inlet was analyzed using the Wind-US code[16]. The Reynolds-averaged Navier-Stokes (RANS) equations were discretized using the Harten /Lax/Van Leer/Contact (HLLC) scheme with a minmod limiter and the SST turbulence model. The equations were solved using an alternating-direction-implicit (ADI) time-marching scheme with a Courant number of 2.0.

Boundary conditions were specified as follows:

- Upstream conditions were supersonic inflow with M = 1.7, and pitch and yaw angles specified.
- Freestream conditions were specified on the outer boundaries.
- The bypass exit was choked to the freestream pressure using a converging-diverging bump on the upper wall.
- The core stream exit pressure was specified for each case to vary the inlet capture ratio. Previous calculations of a coupled inlet and fan showed that the static pressure at the AIP was indeed nearly constant[5].

The solution was initialized to M = 0.6 and run a few hundred iterations to establish subsonic flow in the diffuser. Then the freestream conditions were reset to M = 1.7, and all the external flow blocks were reinitialized. The solution was run 10,000 iterations, which converged the capture ratio and recovery to plotting accuracy.

Subsequent cases were restarted from previous solutions, usually at a higher capture ratio, and run 7,500 – 10,000 iterations to convergence. All calculations were run on a cluster of 11 CPUs running at 3.2 GHz, and took 24–33 hours per case.

V. Comparison of CFD and Test Results

A. Design Point Performance

This section compares the CFD predictions of the dual-stream inlet with the experimental data at the design point, M = 1.7, $\alpha = 0^{\circ}$. First the CFD results are used to describe the overall flow, and then detailed comparisons are made of centerbody pressure distributions, recovery characteristics, and AIP profiles.

Computed Mach number contours along the symmetry plane of the inlet are compared with an overlaid schlieren image in Figure 6. Note that the schlieren optics resolves the effects of the strong lip shock around the entire axisymmetric inlet. This results in an apparent radial shock between the lip and centerbody (at the cut off edge of the schlieren image), while the actual shock curves into the inlet. For this figure the core exit pressure was low, i.e., the MFP was wide open. The schlieren image shows that the cowl captures most of the weak compression

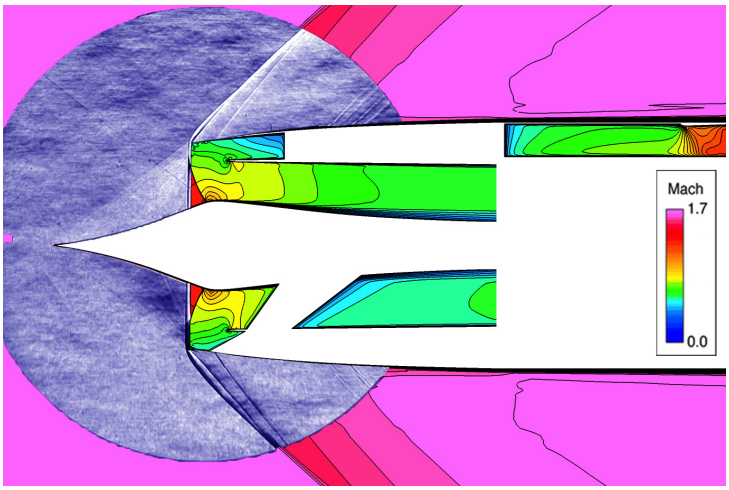

Figure 6. Schlieren image and computed Mach number contours on the inlet symmetry plane, M = 1.7, $\alpha = 0°$.

waves leaving the spike, confirming that the inlet is operating near its full-capture design point. The eight-degree cowl angle generates weak oblique shock waves on the exterior of the inlet, and the normal shock curves far into the inlet. The centerbody boundary layer does not separate, but it does become large (about 20 percent span) at the AIP due to the long subsonic diffuser. The bypass duct is choked to the freestream static pressure at the exit at all supersonic operating points.

Pressure distributions along the centerbody are shown in Figure 7. The CFD solution is at a Mach number of 1.7, but the data was taken at a tunnel Mach number of 1.674. The difference in Mach numbers was accounted for by plotting pressure coefficient

$$Cp = (p - p_\infty)/(p_{0\infty} - p_\infty).$$

The two results are shown at the same capture ratio of about 0.97, indicated by the black diamonds on Figure 8. The CFD and data are in excellent agreement up to the start of the struts at x = 13 inches. As discussed in Section IV A, the wind tunnel model had longer and thicker struts than the flight design analyzed here. The thicker struts in the wind tunnel model leave less area for the flow, and consequently increase the velocity and decrease the pressure below the computed values. Aft of the struts the measurements and CFD are again in good agreement.

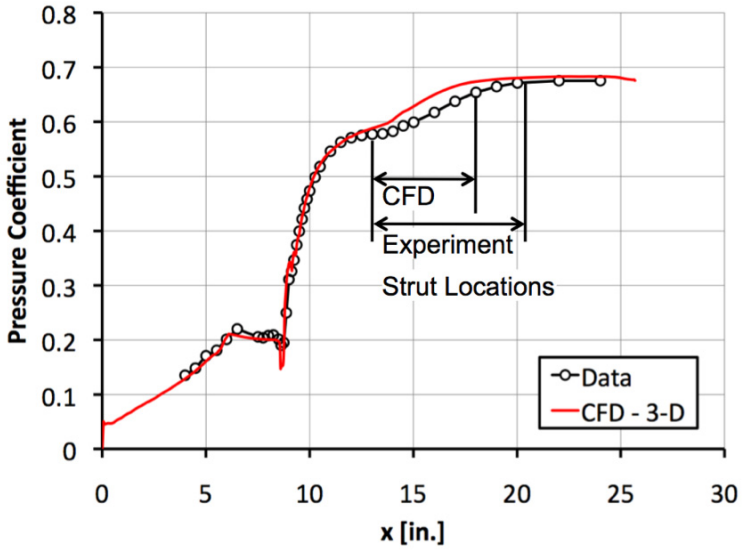

Figure 7. Pressure distribution along the centerbody, M = 1.7, α = 0°.

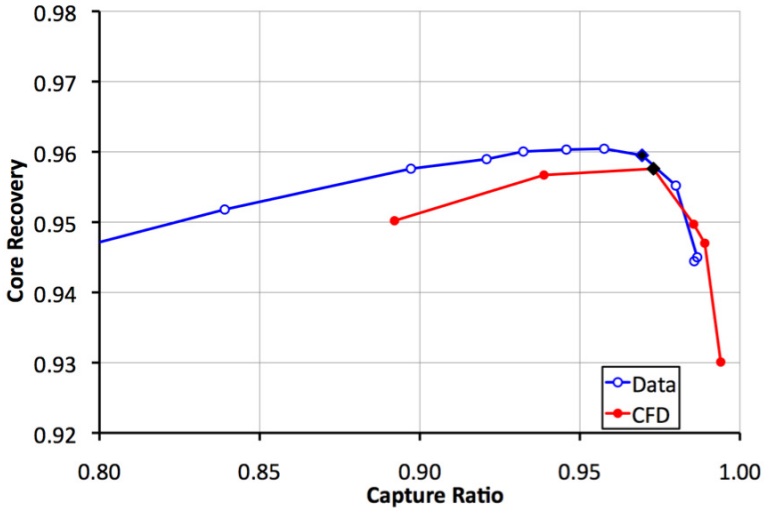

Figure 8. Core recovery vs. capture ratio, M = 1.7, α = 0°.

Overall core total pressure recovery is shown as a function of capture ratio in Figure 8. Capture ratio was varied experimentally by moving the MFP in small increments. The capture ratio was maximum when the MFP was wide open and decreased as the MFP was closed, until the inlet went into buzz at a capture ratio below 0.7 (not shown). AIP total pressures were measured using a standard SAE rake[13] with an additional probe near the hub. Overall recovery was calculated by area-averaging the measured total pressures. The peak recovery was 96 percent, which is 10 percent higher than the normal shock recovery of 0.856 at M = 1.7.

Computations were made at six capture ratios that covered the nominal operating range of the engine on an aircraft. The capture ratio was varied computationally by varying the static pressure at the exit of the core grid. No attempt was made to find the buzz point computationally. The maximum computed capture ratio is slightly higher than the measured value, but, as mentioned previously, the accuracy of the bypass mass flow is uncertain. Computed recoveries were evaluated at the same rake locations, and averaged using the same area-average as the measurements. Computed recoveries are 0.3 – 0.5 percent less than the measured values.

Overall bypass recovery is shown as a function of capture ratio in Figure 9. The computed recoveries were evaluated at the bypass rake probe locations, and overall are 1–1.5 percent lower than the measurements. The discrepancy could be due in part to differences between the tested and modeled geometry discussed earlier, but a more likely cause will be discussed below. For $\alpha = 0°$ the bypass recovery decreases almost linearly with capture ratio. Quite different behavior was seen at $\alpha = 5°$, which will be discussed in Section B, Effects of Angle of Attack.

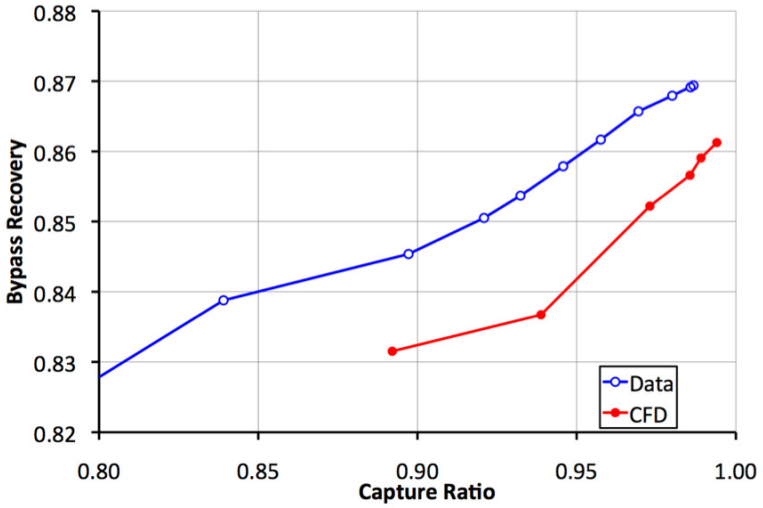

Figure 9. Bypass recovery vs. capture ratio, M = 1.7, α = 0°.

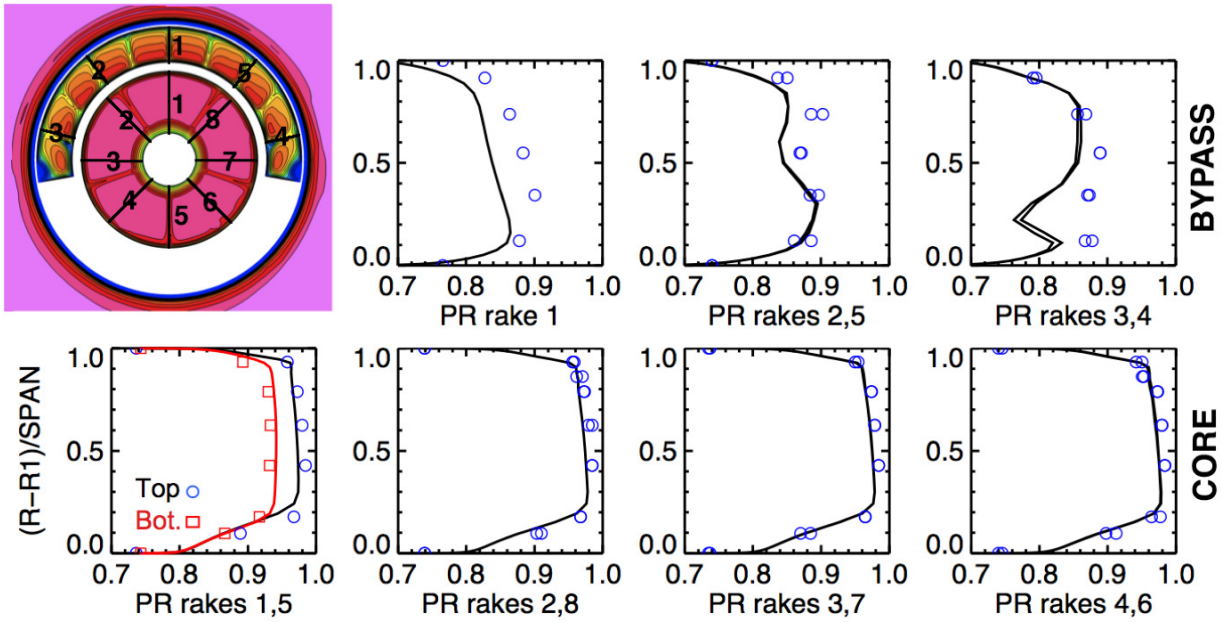

Figure 10. Total pressure recovery contours at the AIP, and profiles at rake locations, M = 1.7, α = 0°.

A comparison of rake profiles reveals the reasons for the discrepancy in bypass recovery noted above. Both the bypass and core rakes were numbered counterclockwise from top dead center, as shown in Figure 10. Computed total pressure recovery contours in that figure show uniform core flow with a thick hub boundary layer and a thin tip boundary layer. This is also seen in the core rake profiles at the bottom of the figure, where symmetric left and right rakes are overlaid. The computed profiles are shown at the same tangential locations as the rakes. The computed profiles are perfectly symmetric, and the computed recoveries are generally one percent less than the measured values.

The plot at the bottom left compares the top and bottom core rakes 1 and 5. Rake 1 is at the top, where the predicted recovery is again about one percent less than was measured. Rake 5 is at the bottom and sits directly in the wake of a centerbody strut. Its measured recovery is 5-6 percent lower than rake 1. In this one location the CFD predicted a higher recovery than was measured. As discussed in Section IV A, the wind tunnel model had longer struts than the flight design modeled with CFD, and would be expected to have a lower recovery than was predicted.

Bypass rake profiles shown along the top of Figure 10 do not agree as well as the core profiles. The bypass rakes all lie directly downstream of long bypass vanes that develop thick wakes. The contour plot shows that bypass rake 1 at the top lies exactly in the center of a wake, and the computed rake recoveries shown at top left are 4-5 percent lower than the data. If the CFD profiles are plotted just outside the wake the agreement with the data is much better, suggesting that the CFD model is not mixing the wake sufficiently with the freestream flow. Wakes from the other bypass vanes cross rakes 2 – 5 at an angle, and the agreement between the CFD and the data varies with radius. In general the computed recoveries are lower than the data, which explains the discrepancy in overall bypass recovery discussed above.

B. Effects of Angle of Attack

The dual-stream inlet was tested at angles of attack between -2° and +5°. Here CFD predictions are compared with the experimental data at α = 5°, an extreme condition that an aircraft would be very unlikely to encounter. First the CFD results are used to describe the overall flow, and then detailed comparisons are made of recovery characteristics and AIP profiles.

Computed Mach number contours along the symmetry plane of the inlet are compared with an overlaid schlieren image in Figure 11. For this figure the core exit pressure was high, i.e., the MFP was partially closed. The weak compression waves from the bottom of the spike are captured inside the cowl, but the waves from the top of the spike spill outside the cowl, confirming that the inlet is operating at a lower capture ratio. The asymmetric bow shock causes the centerbody boundary layer to separate on top. This is apparent in both the schlieren image and the computations.

Computed total pressure recovery contours at the AIP in Figure 12 show the asymmetric wave pattern around the inlet and the thick boundary layer at the top of the centerbody. Thus, operation at angle of attack introduces circumferential distortion at the fan face; however, the distortion is mostly confined to the hub, while modern fans tend to be more sensitive to tip distortion.

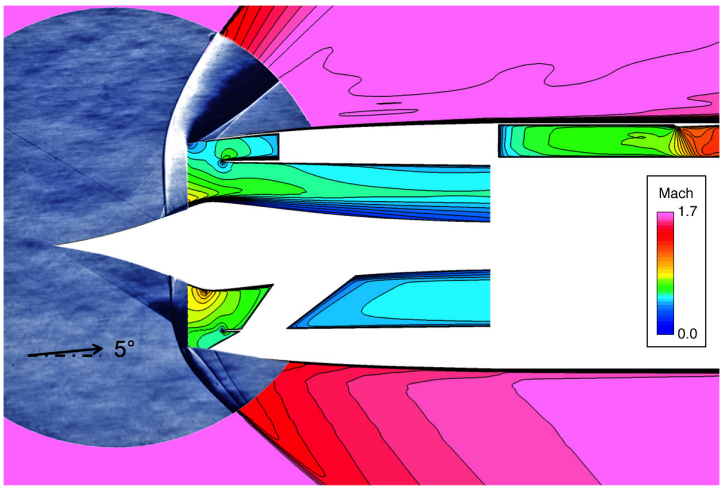

Figure 11. Schlieren image and computed Mach number contours on the inlet symmetry plane, M = 1.7, α = 5°.

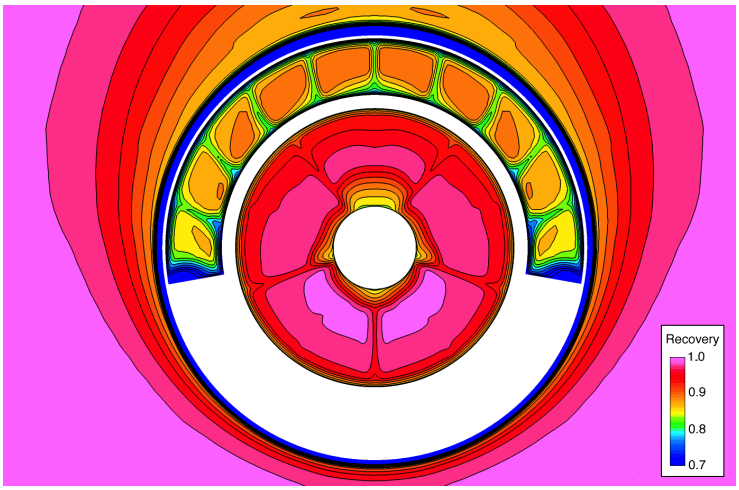

Figure 12. Total pressure recovery contours at the AIP, M = 1.7, α = 5°.

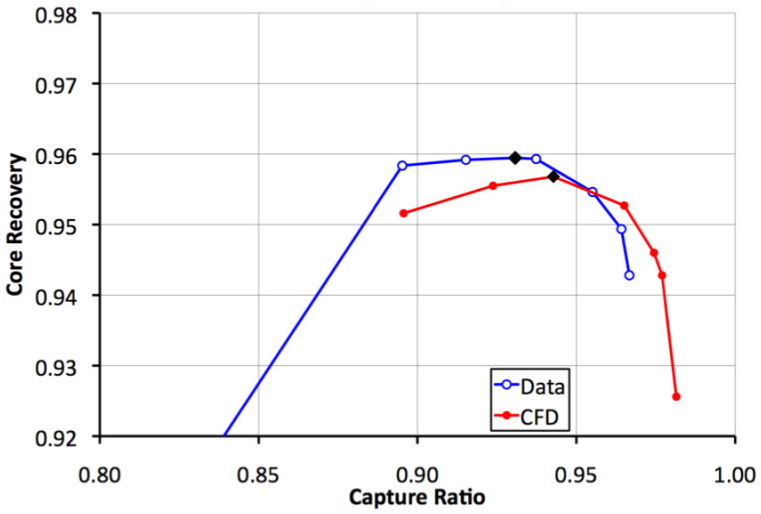

Figure 13. Core recovery vs. capture ratio, M = 1.7, α = 5°.

The overall core total pressure recovery plot shown in Figure 13 is similar to the recovery plot at zero angle of attack shown in Figure 8, but with two significant differences. First, the maximum measured capture ratio has decreased to 96.7 percent due to the spillage over the top of the inlet as noted previously. Second, the measured buzz point has increased from 0.6–0.7 to 0.79–0.89. This is close to the engine operating range, but again, α = 5° is an extreme condition. The reason for the decrease in stable operating range is unknown. The computations are within 0.5 percent of the measurements, and they were completely stable at the lowest capture ratio computed.

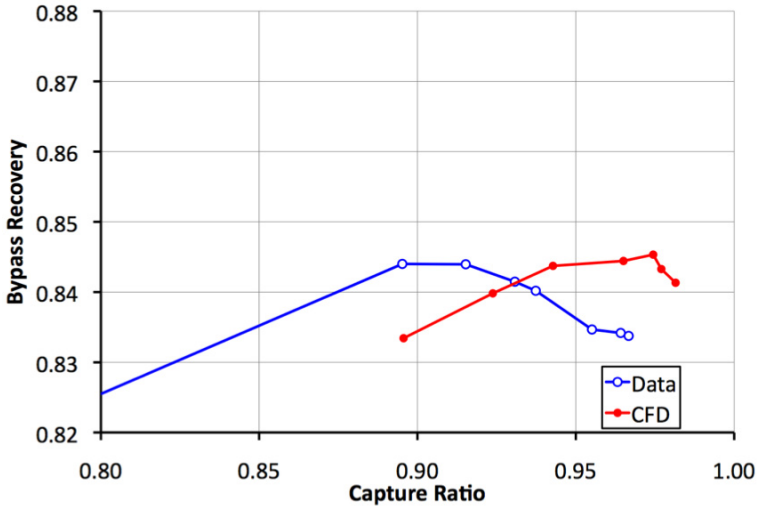

Figure 14. Bypass recovery vs. capture ratio, M = 1.7, α = 5°.

Bypass recoveries for α = 5° shown in Figure 14 behave quite differently than those for Figure 9. At α = 0° the bypass recovery decreases almost linearly with capture ratio, but at α = 5° the measured recovery has a maximum at a capture ratio around 0.90, and the CFD predictions have a maximum at a capture ratio of 0.975. The following discussion examines the CFD predictions to explain the cause of the discrepancy.

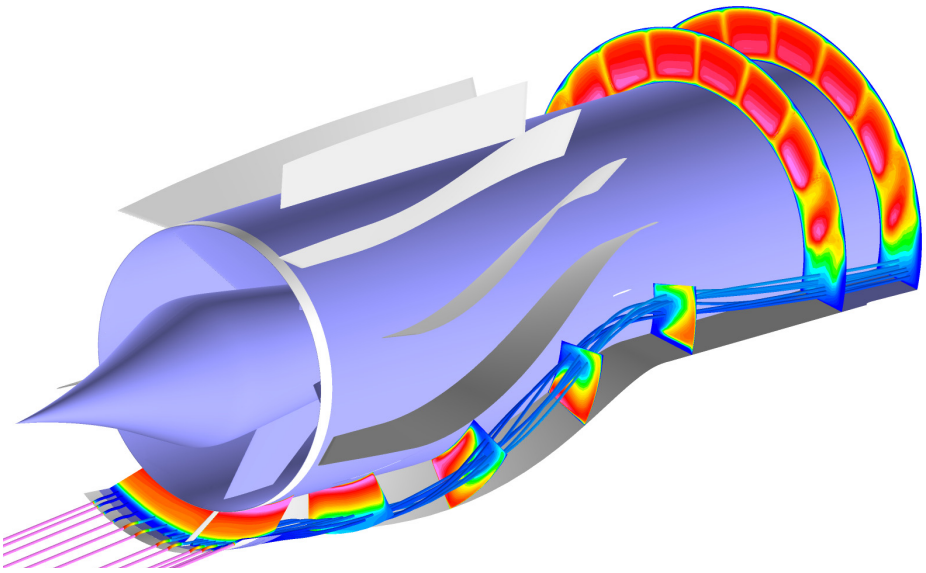

Figure 15. Computed streamlines and recovery contours in the bottom bypass channels, M = 1.7, α = 5°, high capture ratio.

At α = 5° and high capture ratios the CFD solutions showed that the lower (windward) cowl lip was separated, and that the separated flow was confined to the two lower bypass channels. This is illustrated in Figure 15, which shows particle traces and recovery contours in the bottom bypass channels. Particle traces released near the separated cowl lip make one complete revolution around the channel and pass through the lowest recovery regions at each channel cross section. The large lip separation and the strong secondary flows are both challenging flow phenomena for any turbulence model to predict.

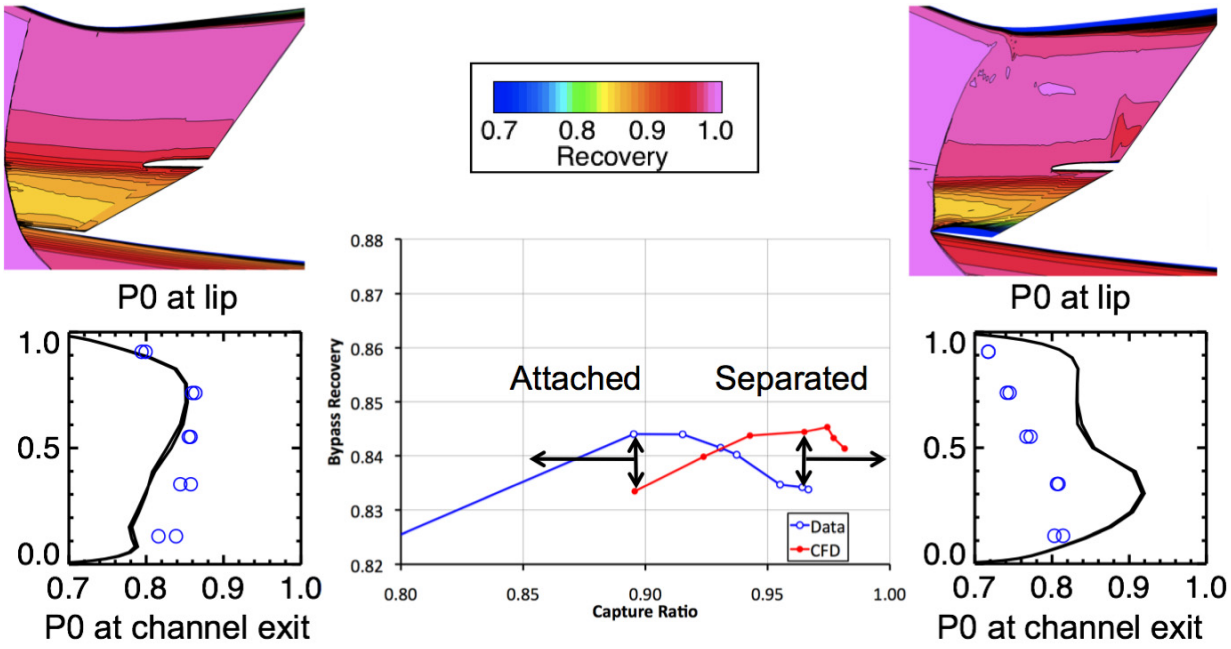

Figure 16. Cowl lip recovery contours and bypass rake profiles at two capture ratios, M = 1.7, α = 5°.

Details of the lip separation at the start of the channel and the bypass recovery at the end of the channel are shown in Figure 16 at $\alpha = 5°$ for both low and high capture ratios. Recovery contours on the center plane near the lower lip are shown at the top, and measured and computed bypass recoveries from the bypass rakes are shown at the bottom. The recovery plot from Figure 14 is repeated in the center for reference.

At low capture ratios (left), the recovery contours show that the bow shock is pushed outside of the inlet, and the flow is attached to the lip. The measured rake profile at the exit of the corresponding bypass channel shows recoveries between 0.8 and 0.86, and the CFD agrees reasonably well. At high capture ratios (right), the recovery contours show that the bow shock is pulled into the inlet, causing the flow to separate from the lip. The measured rake profile at the exit of the corresponding bypass channel shows much lower recoveries between 0.7 and 0.8, suggesting possible separation. Thus, for $\alpha = 5°$ these results suggest the following conclusions:

- At low capture ratios the flow is attached to the lower cowl lip, and the bypass recovery in the bottom channels is similar to the recovery at $\alpha = 0°$, about 84 percent overall. Here the CFD agreement is similar to the results at $\alpha = 0°$.
- At high capture ratios the flow separates at the lower cowl lip, and the bypass recovery in the bottom channels is much lower, about 74 percent overall. Here the CFD over predicts the recovery in the bottom channels, probably because of deficiencies in the turbulence model.

Even though the lower cowl lip separates at high flow and high angle of attack, the CFD results show that the separated flow is captured in the bypass duct, leaving undistorted, high-recovery flow for the engine.

C. Effects of Yaw Angle

The dual-stream inlet was not tested at yaw, but CFD calculations were made to investigate these effects. In this section predictions are shown for $\beta = 5°$, which is also an extreme condition for a commercial aircraft.

Computed symmetry plane Mach number contours for $M = 1.7$, $\beta = 5°$ are shown in a top view in Figure 17. As with angle of attack, compression waves are captured on the windward side of the spike and spilled on the leeward side. Thus the maximum capture ratio also decreases with yaw. The case shown is for a high capture ratio, and, as at angle of attack, the cowl lip separates and the separated flow is captured in the bypass duct. On the windward side the bow shock is pulled far into the core and causes the centerbody flow to separate. The core flow reaccelerates to low supersonic speeds, and then shocks back down to subsonic.

Total pressure recovery contours at the AIP are shown in Figure 18. Bypass channels on the left of the figure have clean flow, but bypass channels on the right show the results of the lip separation. The core flow shows an unusual circumferential distortion pattern at the hub. The effects of this type of distortion on engine operation require further study.

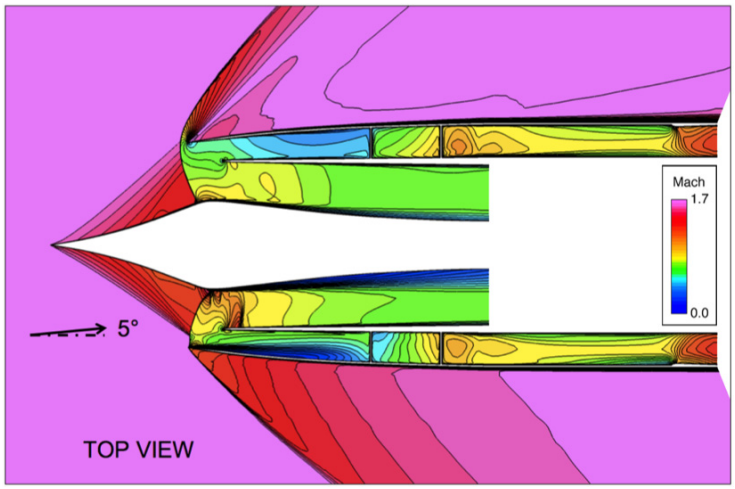

Figure 17. Computed Mach number contours on the inlet symmetry plane, top view, M = 1.7, β = 5°.

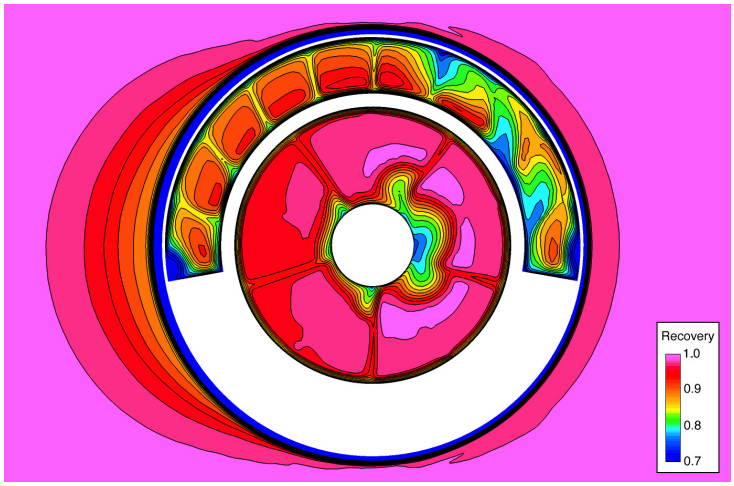

Figure 18. Total pressure recovery contours at the AIP, M = 1.7, β = 5°.

VI. Summary and Conclusions

CFD predictions were made of a low-boom dual-stream inlet, and compared with experimental data. The inlet was designed by engineers at Gulfstream Aerospace Corporation for use on a conceptual small supersonic aircraft, and was tested in the 8x6 foot Supersonic Wind Tunnel at NASA Glenn Research Center.

Test results showed that the dual-stream inlet had excellent performance, with capture ratios near one and peak core total pressure recoveries of 96 percent. The bypass recovery was much lower, between 84 and 87 percent. Gulfstream engineers feel that bypass losses are more than compensated for by gains in boom signature, core recovery, and engine operability. The inlet operated stably over a range of capture ratios much larger than the engine operating range. The peak core recovery remained constant with angle of attack, but the stable operating range decreased.

CFD predictions were made with the Wind-US CFD code, on a grid with nearly 24 million grid points. The HLLC differencing scheme and Menter SST turbulence model were used. Predictions were compared with the experimental data, and the following results were found:

- Computed shock positions agreed well with schlieren images.
- Computed centerline pressures agreed well with measurements, except between the struts where differences between the tested and computed geometries caused differences in pressure distributions.
- CFD calculations gave a slightly higher maximum capture ratio than was measured. However, the accuracy of the measured bypass flow is uncertain.
- Predicted core recoveries were 0.3−0.5 percent lower than measured recoveries.
- Predicted bypass recoveries were 1−1.5 percent lower than measured recoveries, probably due to insufficient mixing of the bypass vane wakes.
- Total pressure profiles at the AIP agreed very well with the measurements in the core, but tended to be low in the bypass duct.
- CFD predicted separation at the cowl lip at high capture ratios and high angles of attack or yaw. The separation is consistent with lower total pressures measured at bypass rakes far downstream. The separation is captured in the bypass ducts and would not affect the operation of an installed engine.

CFD was used heavily to design the dual stream inlet. The good agreement between the CFD predictions and the experimental data shows that minor geometric differences between the flight inlet and the model used in the wind tunnel tests had negligible effects on inlet performance, and validates the use of CFD for future designs.

References

1. Conners, T. R., and Howe, D. C., “Supersonic Inlet Shaping for Dramatic Reductions in Drag and Sonic Boom Strength,” AIAA Paper 2006-30, Jan. 2006.
2. Conners, T. R. and Wayman, T. R., “The Feasibility of a High-Flow Nacelle Bypass for Low Sonic Boom Propulsion System Design,” AIAA 29th Applied Aerodynamics Meeting, June 27-30, 2011 (to be published.)
3. Hirt, S. M., Vyas, M. A., Chima, R. V., Reger, R. W., and Wayman, T. R., "Experimental Investigation of a Large-Scale Low- Boom Inlet Concept," AIAA 29th Applied Aerodynamics Conference, June 27-30, 2011 (to be published.)
4. Chima, R. V., Hirt, S. M., and Reger, R., “Axisymmetric Calculations of a Low-Boom Inlet in a Supersonic Wind Tunnel,” AIAA 29th Applied Aerodynamics Meeting, June 27-30, 2011 (to be published.)
5. Chima, R. V., Conners, T. R., and Wayman, T. R., “Coupled Analysis of an Inlet and Fan for a Quiet Supersonic Jet,” AIAA Paper 2010-479, Jan. 2010. Also NASA TM-2010-216350.
6. Rybalko, M., Loth, E., Chima, R. V., Hirt, S. M., and DeBonis, J. R., “Micro-ramps for External Compression Low-Boom Inlets,” AIAA Paper 2009-4206, June 2009.
7. Rybalko, M. and Loth, E., “Vortex Generators for a Single-Stream Low-Boom Inlet,” AIAA 29th Applied Aerodynamics Conference, June 27-30, 2011 (to be published.)
8. Gillen, T., and Loth, E., “Vortex Generators for a Dual-Stream Low-Boom Inlet,” AIAA 29th Applied Aerodynamics Meeting, June 27-30, 2011 (to be published.)
9. Wilson, J. R., “Quiet Spike Softening the Sonic Boom,” *Aerospace America*, Oct. 2007, pp. 38- 42.
10. Conners, T. R., Merret, J. M., Howe, D. C., Tacina, K. M., and Hirt, S. M., “Wind Tunnel Testing of an Axisymmetric Relaxed External Compression Inlet at Mach 1.97 Design Speed,” AIAA Paper 2007-5066, July, 2007.
11. Hirt, S. M., Tacina, K. M., Conners, T. R., Merret, J. M., and Howe, D. C., “CFD Results for an Axisymmetric Isentropic Relaxed Compression Inlet,” AIAA Paper 2008-0092, Nov. 2008. Also NASA TM-2008-215416.
12. Soeder, R. H., “NASA Lewis 8- by 6-Foot Supersonic Wind Tunnel User Manual,” NASA TM-105771, Feb. 1993.

13. SAE S-16 Committee, ARP 1420, Revision B, "Gas Turbine Inlet Flow Distortion Guidelines," Society of Automotive Engineers, Feb. 2002.
14. Pointwise and Gridgen CFD mesh generation software, Pointwise, Inc., 213 S. Jennings Ave., Fort Worth, TX 76104.
15. Chima, R. V., "TCGRID 3-D Grid Generator for Turbomachinery, User's Manual and Documentation," July, 2003, http://www.grc.nasa.gov/WWW/5810/rvc/docs.htm
16. Towne, C. E., "Wind-US User's Guide, Version 2.0," NASA TM-2009-215804, Oct. 2009.

REPORT DOCUMENTATION PAGE	Form Approved OMB No. 0704-0188

The public reporting burden for this collection of information is estimated to average 1 hour per response, including the time for reviewing instructions, searching existing data sources, gathering and maintaining the data needed, and completing and reviewing the collection of information. Send comments regarding this burden estimate or any other aspect of this collection of information, including suggestions for reducing this burden, to Department of Defense, Washington Headquarters Services, Directorate for Information Operations and Reports (0704-0188), 1215 Jefferson Davis Highway, Suite 1204, Arlington, VA 22202-4302. Respondents should be aware that notwithstanding any other provision of law, no person shall be subject to any penalty for failing to comply with a collection of information if it does not display a currently valid OMB control number.
PLEASE DO NOT RETURN YOUR FORM TO THE ABOVE ADDRESS.

1. REPORT DATE *(DD-MM-YYYY)*	2. REPORT TYPE	3. DATES COVERED *(From - To)*
01-11-2011	Technical Memorandum	

4. TITLE AND SUBTITLE
Computational Analysis of a Low-Boom Supersonic Inlet

5a. CONTRACT NUMBER

5b. GRANT NUMBER

5c. PROGRAM ELEMENT NUMBER

6. AUTHOR(S)
Chima, Rodrick, V.

5d. PROJECT NUMBER

5e. TASK NUMBER

5f. WORK UNIT NUMBER
WBS 984754.02.07.03.13.02

7. PERFORMING ORGANIZATION NAME(S) AND ADDRESS(ES)
National Aeronautics and Space Administration
John H. Glenn Research Center at Lewis Field
Cleveland, Ohio 44135-3191

8. PERFORMING ORGANIZATION REPORT NUMBER
E-17906

9. SPONSORING/MONITORING AGENCY NAME(S) AND ADDRESS(ES)
National Aeronautics and Space Administration
Washington, DC 20546-0001

10. SPONSORING/MONITOR'S ACRONYM(S)
NASA

11. SPONSORING/MONITORING REPORT NUMBER
NASA/TM-2011-217223

12. DISTRIBUTION/AVAILABILITY STATEMENT
Unclassified-Unlimited
Subject Category: 07
Available electronically at http://www.sti.nasa.gov
This publication is available from the NASA Center for AeroSpace Information, 443-757-5802

13. SUPPLEMENTARY NOTES

14. ABSTRACT
A low-boom supersonic inlet was designed for use on a conceptual small supersonic aircraft that would cruise with an over-wing Mach number of 1.7. The inlet was designed to minimize external overpressures, and used a novel bypass duct to divert the highest shock losses around the engine. The Wind-US CFD code was used to predict the effects of capture ratio, struts, bypass design, and angles of attack on inlet performance. The inlet was tested in the 8-ft by 6-ft Supersonic Wind Tunnel at NASA Glenn Research Center. Test results showed that the inlet had excellent performance, with capture ratios near one, a peak core total pressure recovery of 96 percent, and a stable operating range much larger than that of an engine. Predictions generally compared very well with the experimental data, and were used to help interpret some of the experimental results.

15. SUBJECT TERMS
Supersonic flow; Sonic boom; Computational fluid dynamics (CFD); Inlet

16. SECURITY CLASSIFICATION OF:			17. LIMITATION OF ABSTRACT	18. NUMBER OF PAGES	19a. NAME OF RESPONSIBLE PERSON
a. REPORT	b. ABSTRACT	c. THIS PAGE			STI Help Desk (email:help@sti.nasa.gov)
U	U	U	UU	20	19b. TELEPHONE NUMBER *(include area code)* 443-757-5802